



Mitochondrial damage-induced abnormal glucose metabolism with ageing in the hippocampus of APP/PS1 mice

Shijie Li^{1,2} · Yangyang Wang³ · Xiong Zhang⁴ · Xiaomin Xiong³ · Fanlin Zhou^{1,2} · Xiaoju Li^{1,2} · Jianing Fan³ · Xiao Liang³ · Guangxin Li^{1,2} · Yan Peng⁵ · Yu Li^{1,2,6}

Received: 21 August 2022 / Accepted: 23 May 2023 / Published online: 8 June 2023

© The Author(s), under exclusive licence to Springer Science+Business Media, LLC, part of Springer Nature 2023

Abstract

Introduction Accumulation of β -amyloid ($A\beta$) in neurons of patients with Alzheimer's disease (AD) inhibits the activity of key enzymes in mitochondrial metabolic pathways, triggering mitochondrial dysfunction, which plays an important role in the onset and development of AD. Mitophagy is a process whereby dysfunctional or damaged mitochondria are removed from the cell. Aberrant mitochondrial metabolism may hinder mitophagy, promote autophagosome accumulation, and lead to neuronal death.

Objectives The aim of this experiment is to explore the mechanism of neuronal mitochondria damage in the hippocampus of different age APP/PS1 double transgenic AD mice, and to explore the related metabolites and metabolic pathways for further understanding of the pathogenesis, so as to provide new ideas and strategies for the treatment of AD.

Methods In this study, 24 APP/PS1 (APP^{swe}/PSEN1^{dE9}) mice were divided into 3, 6, 9, and 12-month-old groups, and 6-month-old wild-type C57BL/6 mice were as controls. The Morris water maze test was used to evaluate learning and memory. Levels of $A\beta$ were detected by immunohistochemistry. Electron microscopy was used to observe mitochondrial damage and autophagosome accumulation. Western blot was for measuring LC3, P62, PINK1, Parkin, Miro1, and Tom 20 protein expression levels. Gas chromatography coupled with mass spectrometry was used to screen differentially abundant metabolites.

Results The results showed that with the increase of age in APP/PS1 mice, cognitive impairment, hippocampal neuron mitochondrial damage, and autophagosome accumulation all increased. Furthermore, enhanced mitophagy and impaired mitochondrial clearance leading to metabolic abnormalities were observed with ageing in APP/PS1 mouse hippocampus. Especially, abnormal accumulation of succinic acid and citric acid in the Krebs cycle was observed.

Conclusion This study investigated the abnormal glucose metabolism associated with age-related damage to mitochondria in the hippocampus of APP/PS1 mice. These findings provide new insights into the pathogenesis of AD.

Keywords Alzheimer's disease (AD) · Hippocampus · Mitochondrial autophagy · Glucose metabolism; Age

✉ Yu Li
liyu100@cqu.edu.cn

¹ Chongqing University Cancer Hospital, Chongqing 400030, P.R. China

² Chongqing Key Laboratory for Intelligent Oncology in Breast Cancer (ICQBC), Chongqing University Cancer Hospital, Chongqing 400030, P.R. China

³ School of Medicine, Chongqing University, Chongqing 400030, P.R. China

⁴ Basic Medicine College, Chongqing Medical University, Chongqing, P.R. China

⁵ Teaching and Research Section of Pathology and Pathophysiology, School of Basic Medical Science, Chongqing Medical University, Chongqing 400016, P.R. China

⁶ Department of Pathology, Chongqing University Cancer Hospital, Hanyu Road, Shapingba District, Chongqing 400030, China

Abbreviations

AD	Alzheimer's disease
A β	β -amyloid
NFTs	Neurofibrillary tangles
APP	Amyloid precursor protein
ATP	Adenosine triphosphate
LC3	Microtubule-associated protein LC3
TOM20	Translocase of outer membrane 20
PCA	Principal component analysis
P62	Sequestosome 1
<i>PINK1</i>	PTEN-induced putative kinase 1
BCA	Bicinchoninic acid
TEM	Transmission electron microscopy
MWM	Morris water maze test
APP/PS1 double transgenic mice	APP ^{swe} /PSEN1 ^{dE9} (APP/PS1) transgenic Alzheimer's disease model mice

1 Introduction

Alzheimer's disease (AD) is the most common chronic, progressive neurodegenerative disease (Scheltens et al. 2021). The main clinical manifestations of AD are cognitive dysfunction and memory impairment (Ferrari, & Sorbi, 2021). Senile plaques composed of β -amyloid (A β) and neurofibrillary tangles (NFTs) formed by hyperphosphorylation of Tau protein are the main pathological features of AD (2022; Barthelemy et al. 2020). The aetiology of AD is diverse and the pathogenesis is complex (Xiong et al. 2020). Lots of studies have shown that changes in a variety of organelles, such as the mitochondria in hippocampal neurons, are involved in the onset and progression of AD (Fang et al. 2019; Pradeepkiran and Reddy, 2020; Zhou et al. 2020).

Mitochondria are called cellular energy factories, which are essential to life in most organisms (Akbari et al. 2019). Adenosine triphosphate (ATP), the direct supplier of energy in living organisms, is mainly produced by mitochondrial respiration (glycolysis) and the tricarboxylic acid cycle (TCA) in cells (Butterfield & Halliwell, 2019; Tang, 2020; Wang et al., 2020b). The brain has particularly high energy demands and is less tolerant of mitochondrial dysfunction than other tissues (Weidling, & Swerdlow, 2020). In AD, mitochondria are more susceptible to damage due to a lack

of histone protection (Nikolac Perkovic et al. 2021). Mitochondrial damage causes cellular metabolic dysfunction, resulting in neuronal death and increased susceptibility to AD and other related neurodegenerative diseases (John, & Reddy, 2021; Park et al. 2021). Therefore, mitochondrial dysfunction plays a central role in the pathogenesis of AD (Perez Ortiz, & Swerdlow, 2019).

Autophagy is a lysosomal degradation pathway in cells. Damaged organelles and denatured proteins are encapsulated by phagosomes to form autophagosomes, which fuse with lysosomes to form autophagolysosomes that are targeted for biodegradation and recycling (Cen et al. 2020; Luo et al. 2020). Mitophagy refers to the process by which cells remove and recycle damaged or aged mitochondria (Cai & Jeong, 2020; Reddy & Oliver, 2019). It is regulated by the PINK1-Parkin-Miro pathway (Kane, & Youle, 2011). PINK1 is a serine/threonine protein kinase that localizes to the outer mitochondrial membrane (Wang et al. 2020). Parkin is an E3 ubiquitin ligase that is localized to the cytoplasm (Quinn et al. 2020). Miro is mainly localized to the outer mitochondrial membrane and contains two tandem "EF-hand" domains and two different GTPase domains (Panchal, & Tiwari, 2021). In mammalian neurons, healthy mitochondria are linked by Miro protein to form a complex with the kinesin KHC on microtubules, allowing for axonal transport to the cell body (Lopez-Domenech et al. 2018). When mitochondria are damaged, PINK1 activates Parkin and forms a complex with Miro. This complex promotes Miro phosphorylation, resulting in its ubiquitination and degradation. As a result, damaged mitochondria detach from microtubules and undergo mitophagy (Liu et al. 2012). Studies have shown that the autophagy/lysosomal pathway is blocked in CNS neurons of patients with AD (Li et al. 2017). Inhibition of the autophagy/lysosomal pathway in the CSN neurons prevents the removal of damaged mitochondria, leading to the accumulation of abnormal mitochondria. Accumulation of damaged mitochondria further impairs mitophagy, eventually leading to neuron death (Jeong, 2017). Previous reports have shown that patients with AD have severe mitochondrial damage in CNS neurons (Reddy et al. 2018). This damage is indicative of mitochondrial dysfunction and is associated with metabolic changes, such as abnormal glucose metabolism, in the neurons (Eysert et al. 2020).

Studies have shown that the brains of patients with AD utilize less glucose, have reduced rates of glycolysis, and have higher glucose concentrations. These findings suggested that impaired glycolysis and glucose utilization in neurons are basic features of AD (An et al. 2018). Abnormal metabolism in the hippocampus has been previously associated with the progression of AD symptoms (Mahajan et al. 2020). Many studies have focused on autophagy and mitochondrial dysfunction in AD, but dynamic changes in

the PINK1/Parkin/Miro mitophagy pathway have received less attention. In particular, dynamic changes in metabolites produced during mitochondrial damage in neurons have not been evaluated. Therefore, in the present study, age-related changes in cognitive function in APP/PS1 mice, the dynamic processes associated with neuronal mitochondrial damage in the hippocampus, a functional area closely related to cognition, and mitochondrial autoregulation were evaluated. Levels of phagocytosis, expression of proteins in the PINK1/Parkin/Miro pathway, and related metabolites were quantified to further characterize the mechanisms by which mitochondrial damage and changes in energy metabolism interact in AD, to provide insights for the new strategy of AD treatment.

2 Materials and methods

2.1 Mice models and treatments

APP^{swe}/PSEN1^{dE9} double transgenic and wild-type C57BL/6J mice were purchased from Nanjing Junke Biological Engineering Co., Ltd. (animal license number: SCXK[Su] 2015-0001). Mice were housed in the SPF-grade breeding room of the Animal Experiment Center of the Cancer Hospital Affiliated with Chongqing University. Males and females were housed on a 12:12 h light/dark cycle and given free access to food and water. Animal experiments were approved by the Animal Protection and Ethics Committee of Chongqing University Affiliated Cancer Hospital. Mice (N=6/group) were used for behavioural testing, including APP/PS1 mice aged 3, 6, 9, and 12 months and wild-type mice aged 6 months. Transmission electron microscopy, Western blot, and immunohistochemical staining were performed with brain tissue obtained from 3 left hemispheres per group. Gas chromatography-mass spectrometry (GC/MS) was used for metabolite quantification using 5 right hemispheres per group.

2.2 Antibodies and reagents

Rabbit anti-GAPDH and rabbit anti-Tom20 were purchased from Bimake (Shanghai, China). Rabbit anti-LC3B and rabbit anti-P62/SQSTM1 were purchased from Proteintech (USA). Rabbit anti-PINK1, rabbit anti-Parkin, and rabbit anti-Miro1 were purchased from Signalway Antibody (Germany). All secondary antibodies were purchased from Bio-world Technology.

2.3 Morris water maze test

The MWM test was used to assess the learning and memory capabilities of mice. The apparatus was a white circular pool with a diameter of 100 cm and a height of 50 cm. The pool was imaginarily divided into four equal quadrants that were numbered 1, 2, 3, and 4. The fourth quadrant was the target quadrant which contained a cylindrical hidden platform (9 cm diameter, 27 cm height) in its centre. The pool was filled with 23 ± 1 °C water that was made opaque with the addition of nonfat milk powder. Pictures of different shapes, which the mice could use to navigate the maze, were placed on the pool walls of the four quadrants. The experiment included a visual platform test on the first day and a 5-day hidden platform test on the second to sixth days, as well as a probe trial after the last hidden platform test. In the visible platform test, mice were evaluated in four contiguous trials with an intertrial interval of 30 min. In the hidden platform tests, mice were trained for four trials with an intertrial interval of 1 h. Mouse movement was tracked with a Video-Mot2 image analyzer (SANS SA201, China).

2.4 Tissue preparation

Anaesthetize all mice with 1–2% isoflurane because it is safe, has minimal interference with the experiment, does not affect its myocardial function and reduces mouse suffering. Perfusion was cold 0.9% saline solution or cold 0.9% saline solution with 4% polyformaldehyde (PFA). Saline-perfused brain tissues were extracted and preserved at -80 °C until further use. PFA-fixed brain tissues were fixed in 4 °C PFA overnight and embedded in paraffin. Serial coronal hippocampal Sect. (5 µm) were obtained using a conventional surgical microtome (THERMO, HM325).

2.5 Transmission electron microscopy

Brain tissues were prefixed with 3% glutaraldehyde, then postfixated in 1% osmium tetroxide, dehydrated in series acetone, infiltrated in Epox 812, and embedded. Semi-thin sections were stained with methylene blue and ultrathin sections were cut with a diamond knife and stained with uranyl acetate and lead citrate. Sections were examined using a JEM-1400-FLASH TEM.

2.6 Western blot assay

Hippocampal tissue samples were lysed in cold RIPA pyrolysis buffer (Beyotime, China) and PMSF. Protein concentration was determined using a BCA Protein Assay Kit (Beyotime, China) at 570 nm. Unify the sample protein concentration to 5 µg/µl. Add the protein solution to the

sample buffer in a ratio of 1:5 and mix well, denature at 100 °C for 5 min. Store at -80 °C. Equal amounts of protein were loaded into each lane of an SDS-PAGE Bis-Tris gel and transferred to polyvinylidene difluoride (PVDF) membranes (Millipore, Billerica, MS, USA). PVDF membranes were washed with blotting buffer (Tris-buffered saline containing 0.1% Tween-20) and then blocked for 120 min a buffer containing 5% non-fat powdered milk. After three washes with blotting buffer, the PVDF membrane was incubated with primary antibody at 4 °C overnight. After additional washes in the blotting buffer, the PVDF membrane was incubated with a secondary antibody for 40 min at room temperature. Finally, the PVDF membranes were developed with ECL Western Blotting Detection Reagents, and protein expression was quantified with Image J.

2.7 Immunohistochemistry

Samples were permeabilized with 0.2% Triton X-100 for 10 min at room temperature. Normal goat serum was added to the slides and incubated for 30 min at room temperature. The staining protocol employed a modified streptavidin-HRP immunohistochemistry procedure (CoWin Century Biotechnology, Inc, China). Briefly, sections were incubated with primary antibody overnight at 4 °C in a humid box. The next morning, the slides were washed three times with PBST, treated with peroxidase-conjugated streptavidin, and visualized using the diaminobenzidine (DAB) Kit (CoWin Century Biotechnology, Inc, China). Sections were counterstained with hematoxylin. Finally, slides were sealed with neutral gum and observed using a Nikon optical microscope.

2.8 Methyl chloroformate (MCF) derivatization and gas chromatography-mass spectrometry (GC – MS) analysis

To extract metabolites from the brain, the cerebral cortex was first eliminated from the outer surface of the hippocampus. After adding 500 µl of cold methanol-water (50% v/v), tissues were homogenized and centrifuged (17,000 g, 15 min) to collect the supernatant. Hippocampal tissue supernatants were dried via speedVac (Labconco, Kansas, USA) and stored at -20 °C, before to derivatization. The dried supernatants were resuspended in 200 µl of 1 M NaOH and transferred to silanized glass tubes. The MCF derivatized metabolites were analyzed using an Agilent GC7890B System (Agilent Technologies, Inc.) coupled to an MSD5977A mass spectrometer (Agilent Technologies, Inc.), with electron impact ionization at 70 eV. The gas chromatograph was equipped with a Zebron ZB-1701 Capillary GC column (30 m × 250 µm id × 0.15 µm, 5 m guard column; Phenomenex). The derivatized sample (1 µl)

was injected into the GC, which was operated in a split-less mode at 250 °C. Advanced Heatmap Plots were performed using the OmicStudio tools at <https://www.omicstudio.cn>.

2.9 Statistical analysis

All statistical analyses were conducted using SPSS software (version 26.0). The data are expressed as the mean ± standard error of the mean (SEM). Two-way analysis of variance (ANOVA) was used for statistical comparison, followed by Bonferroni's post-test with multiple comparisons. Quantitative analysis was carried out with the help of IMAGE software (version 1.44 P, USA). Metabolomics Standards Initiative metabolite identification was achieved by comparing the mass spectra of fragments with those of an in-house MCF mass spectral library (generated using standards) within an associated retention time window of 1 min. The relative concentrations of the metabolites were calculated using the in-house XCMS-based R script by identifying the most abundant fragment ion within an accurate retention time window. The metabolite concentrations were normalized to the levels of 2,3,3,3-d4- alanine and total protein to correct for dilution effects. PCA was conducted using the Metaboanalyst 3.0 package for R. A false discovery rate (q value) was used to account for multiple comparisons. $P < 0.05$ and $q < 0.05$ indicated a significant difference. Heat maps were generated using ggplot 2 R packages. The difference was significant at $P < 0.05$.

3 Results

3.1 Learning and memory declined with age in the APP/PS1 mice

On days 1–5 of the location-navigation experiment, the mean escape latency of all mice decreased significantly as the number of training days increased ($P < 0.01$). The mean escape latency of the mice in the APP/PS1-9 M and APP/PS1-12 M groups was significantly higher than that in the wild-type ($P < 0.01$) (Fig. 1B). On day 6 of the space exploration experiment, the number of platform crossings in the APP/PS1-9 M and APP/PS1-12 M groups was significantly lower than that in the wild type group ($P < 0.01$) (Fig. 1C). The percentage of time in the NE quadrant was significantly higher in the APP/PS1-6 M, APP/PS1-9 M, and APP/PS1-12 M groups compared to the wild-type group ($P < 0.05$) (Fig. 1D). Learning and memory in the APP/PS1 mice decreased significantly in an age-dependent manner. Figure 1E showed that there was no significant difference in average swimming speed among the mice in each group

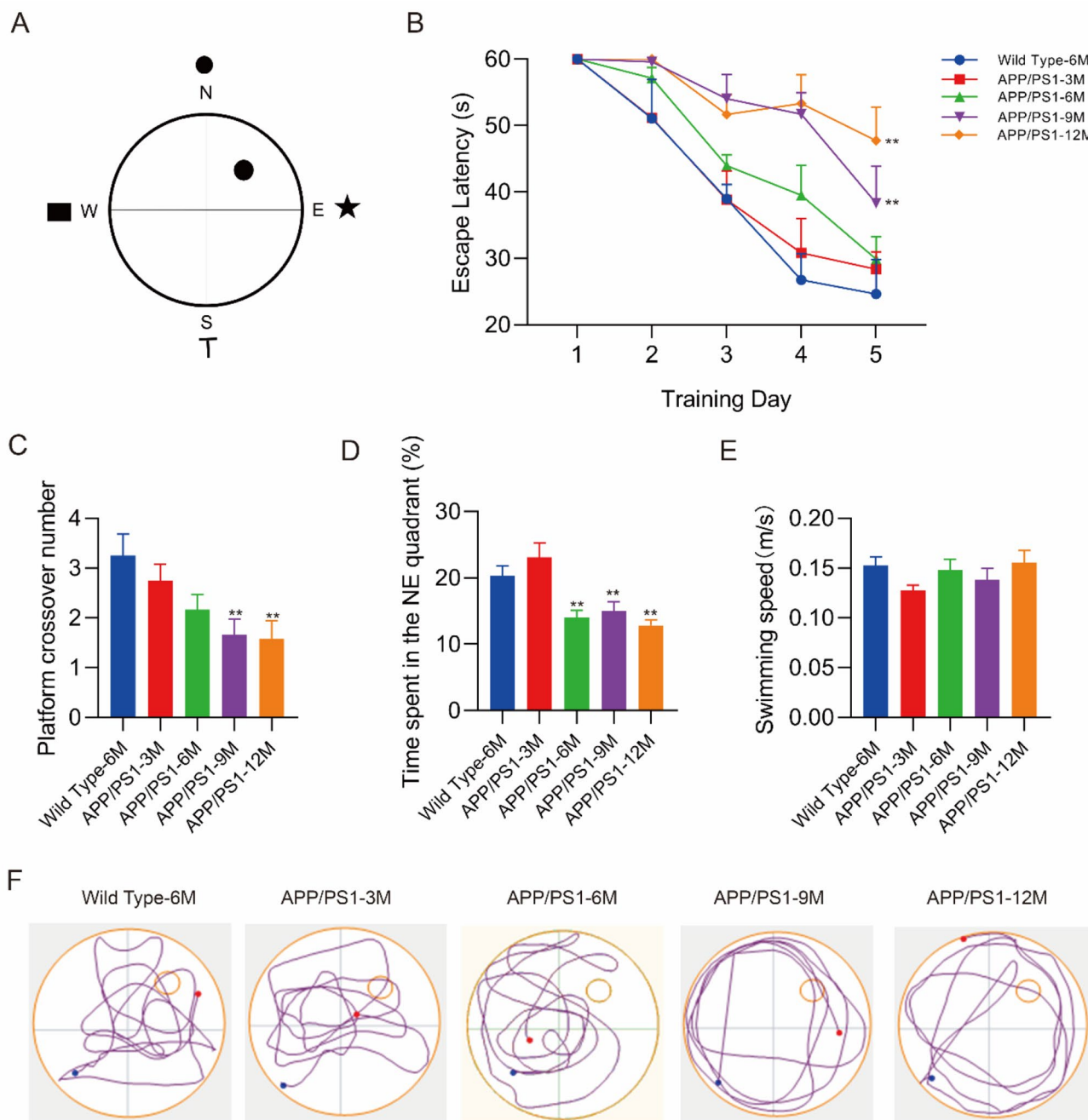


Fig. 1 Loss of learning and memory abilities with advancing age in APP/PS1 mice. **(A)** Schematic diagram of the water maze. **(B)** Comparison of escape latencies in each group of mice in the positioning navigation experiment. APP/PS1-9 M and APP/PS1-12 M groups take longer to reach the submerged platform. **(C)** Comparison of the number of times the mice in each group crossed the platform in the space exploration experiment. APP/PS1-9 M and APP/PS1-12 M groups fail to show a preference for the target platform location. **(D)** Com-

parison of the time that each group of mice spent in the NE quadrant. **(E)** Mean useful velocity for each group of mice. The average swim speed was unchanged in each group. **(F)** The route trajectories of mice in each group crossing the platform in the space exploration experiment. (N=6. Data are shown as the mean \pm SEM. * $P < 0.05$, ** $P < 0.01$, versus wild-type.)

parison of the time that each group of mice spent in the NE quadrant. APP/PS1-6 M, APP/PS1-9 M, and APP/PS1-12 M groups spend less time in the target quadrant compared with the wild-type group. **(E)** Mean useful velocity for each group of mice. The average swim speed was unchanged in each group. **(F)** The route trajectories of mice in each group crossing the platform in the space exploration experiment. (N=6. Data are shown as the mean \pm SEM. * $P < 0.05$, ** $P < 0.01$, versus wild-type.)

3.2 β -amyloid, mitochondrial damage, and autophagosome accumulation in the hippocampus of APP/PS1 mice progressively increased with age

Behavioural tests showed that the experimental group had reduced learning and memory functions. Abnormal changes in the hippocampus, a brain structure closely related to memory, also occurred; more specifically, structural abnormalities in the mitochondria, which are important for energy supply, were observed. A β expression was measured in each mouse group (Fig. 2A), and transmission electron microscopy (TEM) was used to observe subcellular changes in the hippocampal neurons of mice in each group. The nuclei of neurons in the wild-type group were large and round, centrally located in the cell, possessed little chromatin, had complete nucleoli, and clear nuclear membranes. Wild-type neuronal cell membranes were continuous and complete, and a transparent, jelly-like substance was observed in the cytoplasm. The mitochondrial matrix was uniform and filled with densely arranged and regularly distributed cristae (shown in M). No obvious accumulation of autophagosomes was observed. There were no significant differences between the APP/PS1-3 M group and the wild-type group, and the mitochondria were densely arranged with regularly distributed cristae (shown in M). There was no obvious accumulation of autophagosomes in either group. In the APP/PS1-6 M group, the shapes of the nuclei were irregular, and the nuclear membranes were clear near the edge of the cell. The cytoplasm was transparent. The mitochondria showed transparent, oedema-like changes, cristae were broken, and the mitochondrial matrix density was decreased (shown in M). No obvious autophagy was observed in APP/PS1-6 M. In the APP/PS1-9 M group, the nuclear membrane was not clear, and the boundary with the cell membrane was obscured. Chromatin was coarse. The mitochondrial structure was not clear, and there was an obvious accumulation of autophagosomes (indicated by arrows). In the APP/PS1-12 M group, the shape of the nucleus was irregular, the edges of the nuclear membrane and the cell membrane were not clear, the chromatin was coarse, and the mitochondrial structure was not clear. There was an obvious accumulation of autophagosomes (indicated by arrows) in APP/PS1-12 M. These results showed that increasing age in APP/PS1 mice is associated with progressively severe mitochondrial damage and autophagosome accumulation in hippocampal neurons (Fig. 2B).

3.3 Mitochondrial autophagy was increased, and autophagy was inhibited in the hippocampus of APP/PS1 mice with advancing age, resulting in impaired mitochondrial clearance

LC3 protein is an autophagy marker, and P62 protein is a marker of autophagy substrates. Expression levels of LC3II/GAPDH in the APP/PS1-6 M, APP/PS1-9 M, and APP/PS1-12 M groups were significantly higher than those in

the wild-type group ($P < 0.05$) (Fig. 3A). Compared with the wild-type group, P62 protein in the APP/PS1-3 M, APP/PS1-6 M, APP/PS1-9 M, and APP/PS1-12 M groups was significantly increased ($P < 0.05$) (Fig. 3B). These results indicate that the level of LC3-mediated autophagy increased in the hippocampal neurons of APP/PS1 mice with advancing age, but P62 degradation was reduced, indicating that autophagy was hindered.

The effects of AD on mitophagy were evaluated. Compared with the wild-type group, the expression of PINK1 protein in the APP/PS1-3 M, APP/PS1-6 M, APP/PS1-9 M, and APP/PS1-12 M groups was significantly enhanced ($P < 0.01$) (Fig. 3C). In addition, Parkin protein expression in the APP/PS1-6 M, APP/PS1-9 M, and APP/PS1-12 M groups was significantly higher than that in the wild-type group ($P < 0.01$) (Fig. 3D). The expression of Miro1 protein in the APP/PS1-6 M, APP/PS1-9 M, and APP/PS1-12 M groups was significantly decreased compared with that in the wild-type group ($P < 0.01$) (Fig. 3E). These results indicate that mitophagy was enhanced in APP/PS1 mice. There was no significant difference in the expression of Tom 20 protein between the APP/PS1-3 M, APP/PS1-6 M, APP/PS1-9 M, and APP/PS1-12 M groups and the wild-type group ($P > 0.05$) (Fig. 3F). Thus, damaged mitochondria were not effectively removed.

3.4 Disorders of hippocampal metabolism in APP/PS1 mice with advancing age

The experimental groups exhibited memory loss, damaged hippocampal mitochondria, and impaired clearance of damaged cellular material. These mitochondrial abnormalities may affect the production of ATP, which is the primary energy substrate produced by mitochondria. Metabolites of mitochondrial energetics processes were detected using metabolomic methods.

First, principal component analysis (PCA) was performed in hippocampal samples from each treatment group (Fig. 4A). Results showed good repeatability within grouped samples. The detected metabolites were subjected to log₂-transformed heatmap cluster analysis. Compared with the wild-type group, the levels of most metabolites in the APP/PS1-9 M group were significantly increased, and the levels of most metabolites in the APP/PS1-12 M group were significantly decreased (Fig. 4B). These results showed that levels of mitochondrial metabolites changed with age in APP/PS1 mice.

Differential screening of metabolites was performed, and the results are presented as heatmap classifications (Fig. 4C). Compared with the wild-type group, the differential metabolites that decreased in abundance in the APP/PS1-3 M group were D-ribose, myristic acid, n-heneicosanoic acid,

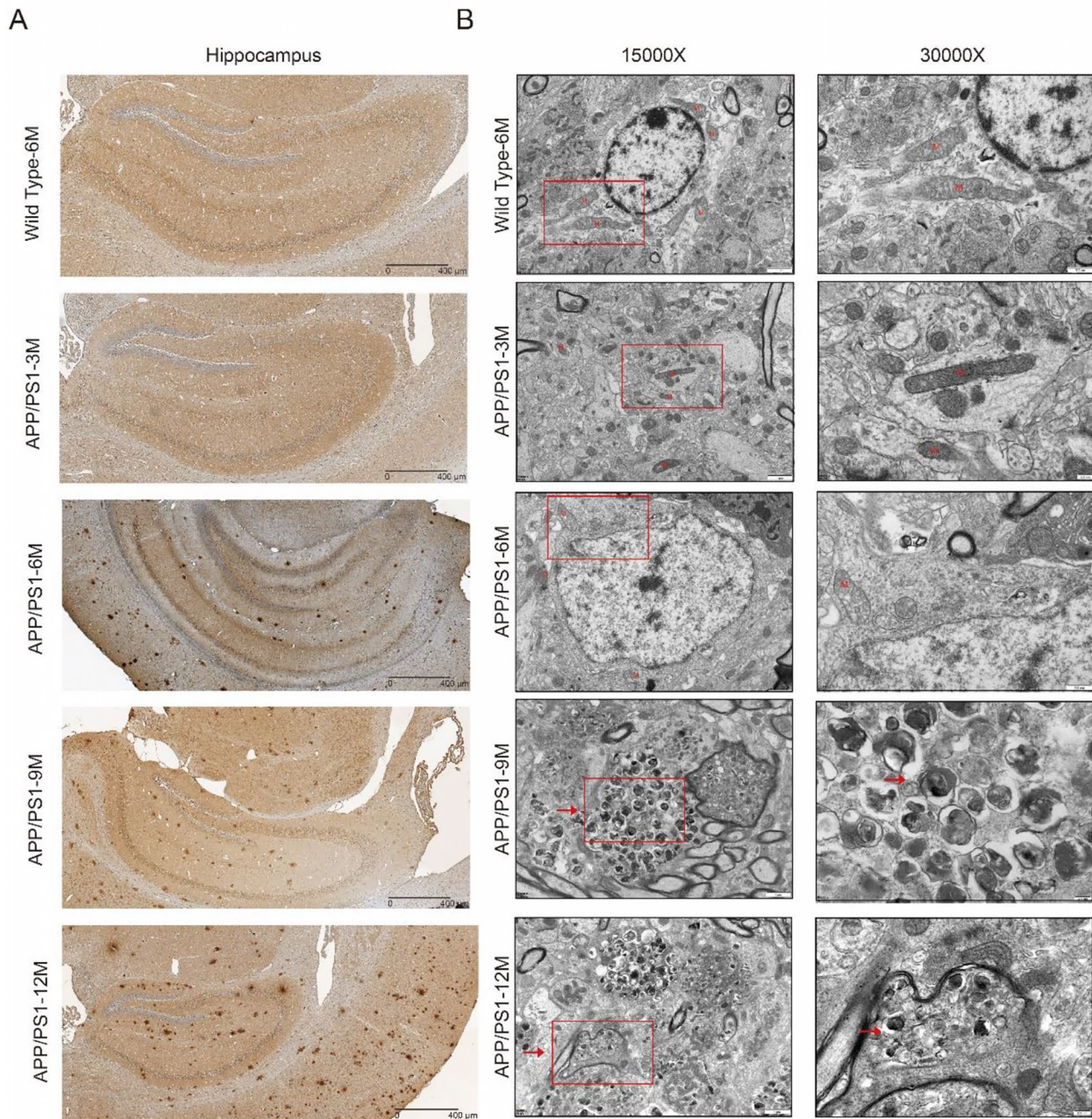


Fig. 2 Mitochondrial damage, accumulation of β -amyloid and autophagosomes in the hippocampus of APP/PS1 mice by age. **(A)** Immunohistochemical expression of β -amyloid in the hippocampus of mice in each group. Wild type-6 M and APP/PS1-3 M: negative staining of β -amyloid in the hippocampus. APP/PS1-6 M: mild compact deposits of β -amyloid in the hippocampus. APP/PS1-9 M: sparse neurofibrillary plaques of β -amyloid in the hippocampus. APP/PS1-12 M: diffuse plaques of β -amyloid in the hippocampus. (Scale bar = 400 μ m.) **(B)** Electron microscopy was used to observe mitochondrial damage and autophagosome accumulation in the hippocampus of mice in each

group at 15000X (left) and 30000X (right). Wild type-6 M and APP/PS1-3 M: mitochondrial structure completion and no obvious accumulation of autophagosomes. APP/PS1-6 M: edematous changes in mitochondrial structure and no obvious accumulation of autophagosomes. APP/PS1-9 M: APP/PS1-9 M: the mitochondrial structure was not clear and there was an accumulation of autophagosomes. APP/PS1-12 M: mitochondrial structural damage and obvious accumulation of autophagosomes. (M: Mitochondrion. Arrows: Autophagosome. Frame: The enlarged part.)

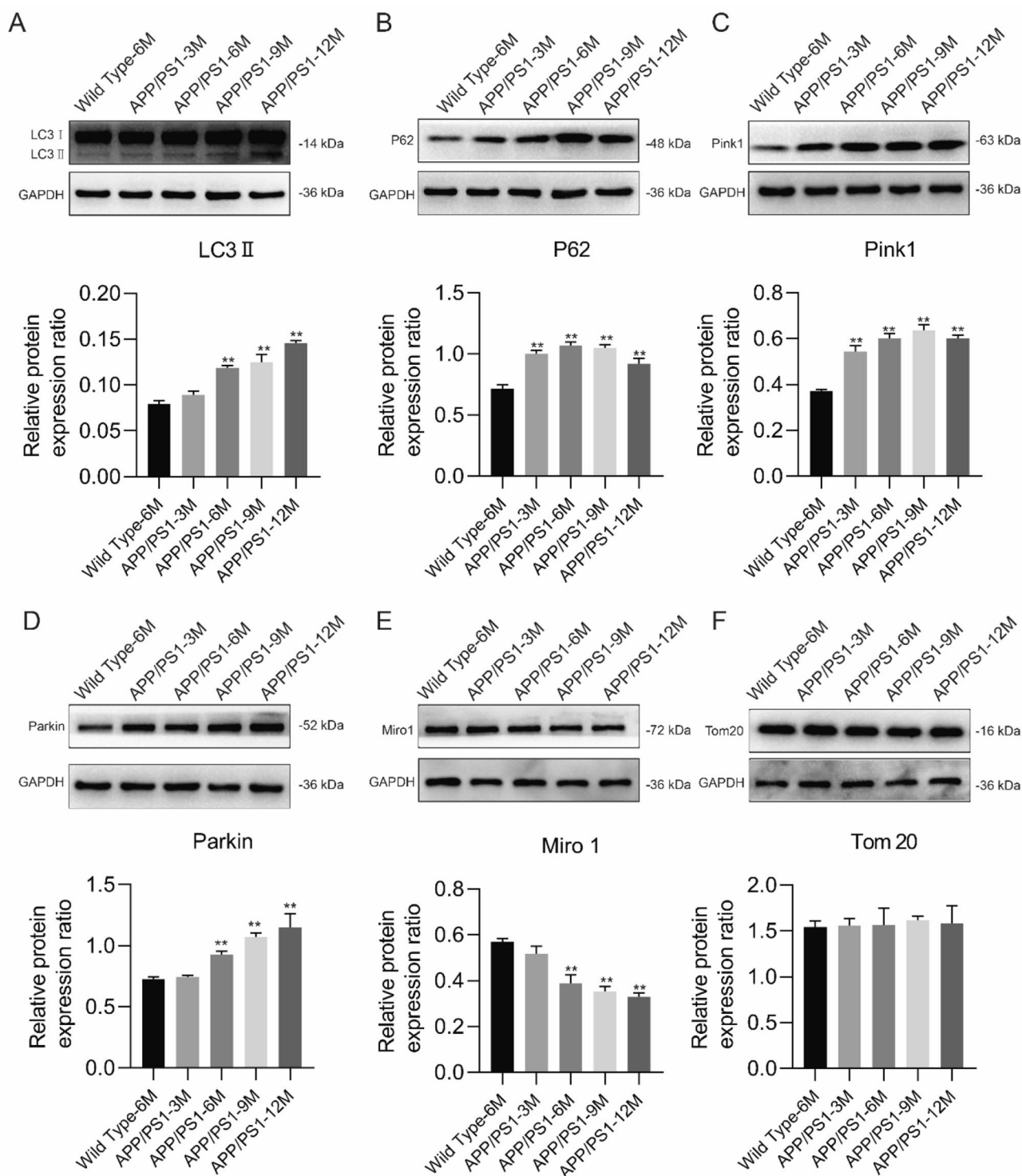


Fig. 3 Increased mitophagy, suppressed autophagy, and impaired mitochondrial function in the hippocampus of APP/PS1 mice with advancing age. **A–F)** Protein expression and optical density analysis of LC3II, P62, Pink1, Parkin, Miro1, Tom20 in the hippocampus of mice in each group. **(A–D)** Compared with the wild-type group, the relative expression of protein LC3, P62, Pink1 and Parkin significantly increased

in APP/PS1 group. ($P < 0.05$) **(E)** The relative expression of protein Miro1 was significantly decreased in APP/PS1 group. ($P < 0.05$) **(F)** The relative expression of protein Tom20 has no significant difference. ($N = 5$. Data are shown as the mean \pm SEM. * $P < 0.05$, ** $P < 0.01$, versus wild-type.)

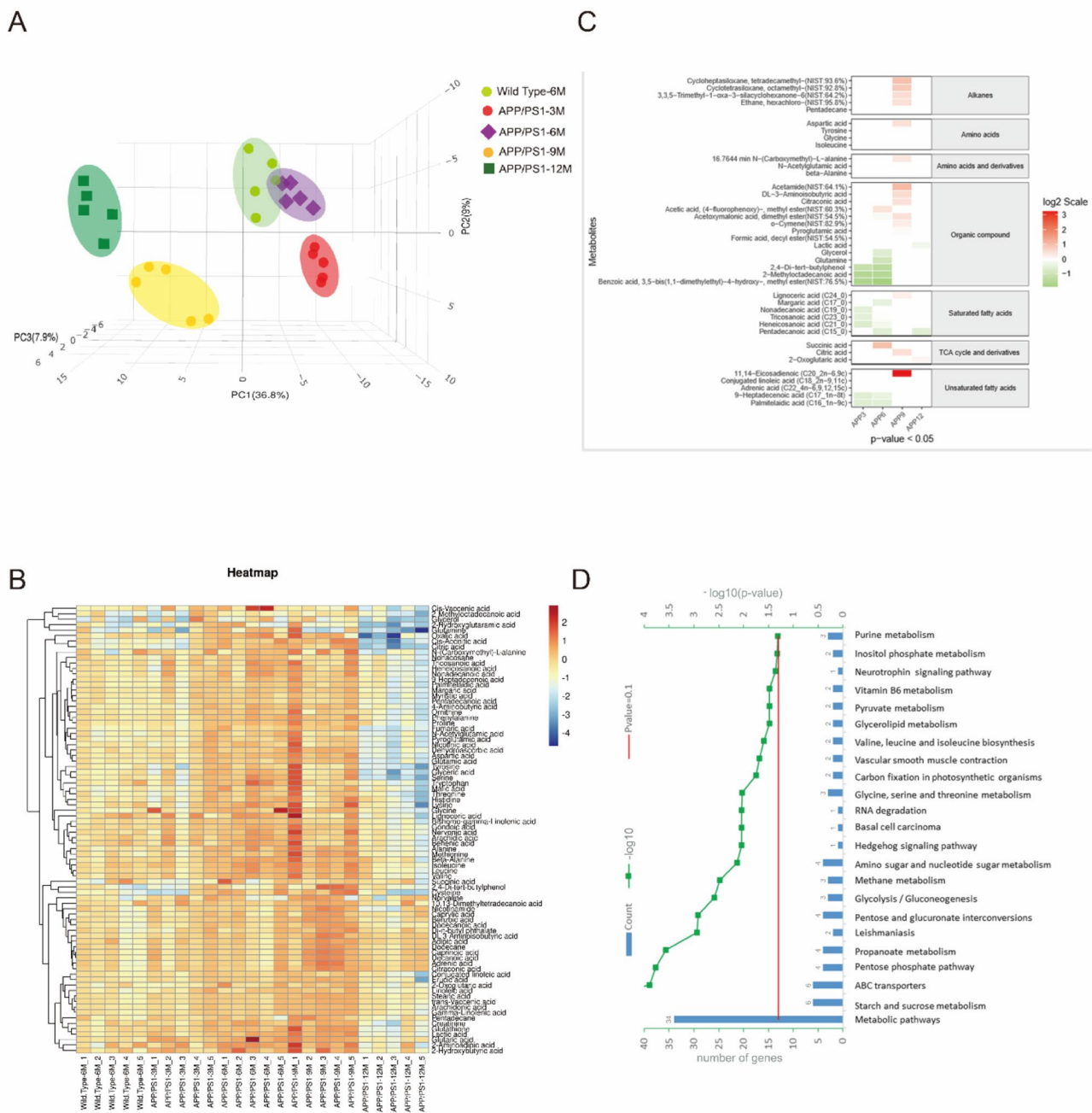


Fig. 4 Metabolite disorders in the hippocampus of APP/PS1 mice with advancing age. **(A)** Analysis of 3D dimensionality reduction using PCA of the sequence- and structure-based descriptors present in FC-1 to FC-3. FC-1 shows a contribution of explained variance ratio of 36.8% (PC1), 9% (PC2), and 7.9 (PC3). **(B)** Clustering heatmap of mice in each group. Each row represents a metabolite, and each column represents the sample tested. The colour key indicates the expression level of the metabolite, red represents metabolite with an expression level above the mean, and green represents metabolite with an expression level below the mean. **(C)** Predicted metabolic pathway activities for

APP/PS1 mice. Red blocks represent higher predicted metabolite levels, whereas green blocks represent lower predicted metabolite levels. Only the metabolic pathways with p-value and q-value less than 0.05 are displayed in the heatmap. **(D)** KEGG pathway diagram for the hippocampus of APP/PS1 double transgenic mice. The 23 KEGG pathways from the KEGG enrichment results are displayed. The abscissa is the KEGG pathway, and the ordinate is the significance level of pathway enrichment. The higher the value, the greater the significance. (N = 5. Data are shown as the mean \pm SEM, versus wild-type.)

and tricosanoic acid ($P < 0.05$). Glutamine, isoleucine, margaric acid, and pentadecanoic acid levels were significantly decreased in the APP/PS1-6 M group ($P < 0.05$). The differential metabolites that increased in abundance in the APP/PS1-6 M group were succinic acid and acetic acid. In the APP/PS1-9 M group, aspartic acid, citric acid, lignoceric acid, DL-acetyl glutamic acid, and pyroglutamic acid levels were increased ($P < 0.05$). In the APP/PS1-12 M group, the levels of 2-oxoglutaric acid and lactic acid were decreased ($P < 0.05$). These results show that succinic acid and citric acid, which are key metabolites in the TCA cycle, changed with age in APP/PS1 mice.

Associated metabolic pathways of differentially abundant metabolites were determined by Associated metabolic pathways of differentially abundant metabolites were determined using the Kyoto Encyclopedia of Genes and Genomes (KEGG) (Fig. 4D). The metabolic pathways associated with differentially abundant metabolites in APP/PS1 mice mainly included purine, pyruvate, threonine, glycine, isoleucine, glycolysis, gluconeogenesis, and pentose phosphate. Among these, the main pathway related to mitochondrial ATP production is glycolysis.

4 Discussion

The 20th-century German scientist Alois Alzheimer discovered and named AD when dissecting a patient with severe memory deficits. AD is a chronic, progressive neurodegenerative disease characterized by amyloid plaques and NFTs, in which clearance of A β has long been the focus of research (Tolar et al. 2020).

The most commonly used in vivo model of AD is the APP^{swe}/PS1 Δ E9 double transgenic mouse. This transgenic mouse can stably express the A β precursor protein APP, which degrades to generate insoluble A β . In this model, the expression level of APP increases with age, resulting in A β accumulation (Zhao et al. 2020). Here, the MWM test was used to monitor age-dependent changes in hippocampus-dependent learning and memory abilities of APP/PS1 double-transgenic mice (Lonnemann et al. 2020). The results showed that the average escape latency of APP/PS1 double-transgenic mice at 9 and 12 months was significantly increased compared to that in the control group. In addition, the number of platform area crossings was significantly reduced in 9 and 12-month-old APP/PS1 mice compared to that in controls. The swimming distance and swimming speed did not differ significantly between the groups. These results indicated that the learning and memory ability of APP/PS1 mice decreased with age, but the motor ability was not affected. This finding was consistent with a previous

study that showed progressive age-dependent impairment of cognitive function in mice (Velazquez et al. 2019).

The hippocampus is a key brain region responsible for learning and memory. Changes in neurons in the hippocampus, including reduced synaptic density and impaired synaptic transmission, were presented in the early stages of AD and ultimately lead to learning and memory impairment (Babcock et al. 2021). Studies have reported that neuronal changes in the early stages of AD were closely related to damage in the mitochondria, which were key organelles that support synaptic function and mitigate synaptic stress (Shoshan-Barmatz et al. 2018). Mitochondrial damage includes changes in mitochondrial morphology and number, and mitochondrial autophagy dysfunction (Hou et al. 2019). Mitochondrial changes include a decrease in the number of mitochondria, a shorter and wider shape, disappearance of the bilayer membrane structure, irregular dorsal cristae of the inner mitochondrial membrane, and oedema of the mitochondrial matrix (Swerdlow, 2018). Abnormalities in mitophagy include abnormal initiation of mitophagy, accumulation of autophagolysosomes, and abnormal lysosomal degradation (Sun et al. 2021).

In the present study, the experimental APP/PS1 mice had decreased numbers of mitochondria, altered mitochondrial shape, and mitochondrial oedema at 6 months-of-age. The mitochondrial shape was unclear at 9 and 12 months-of-age in experimental APP/PS1 mice, and autophagosome accumulation was evident. Mitochondrial damage in the hippocampus correlated with memory deficits in experimental APP/PS1 mice at 9 months-of-age, consistent with the findings of previous studies (Jadiya et al. 2019). To further characterize the relationship between mitochondrial damage and autophagy, the expression levels of the canonical PINK1/Parkin/Miro mitophagy pathway were measured using Western blot (Lopez-Domenech et al. 2021). PINK1 is located upstream of Parkin in normal mammalian neurons, and the Miro protein is involved in mitochondrial axonal transport (Imai, 2020). When mitochondria are damaged, PINK1 activates Parkin and activated Parkin recruits and promotes the degradation of Miro, allowing damaged mitochondria to detach from microtubules in order to undergo mitophagy (Bharat, & Wang, 2020). In the present study, PINK1 protein expression was significantly increased at 9 and 12 months-of-age in the experimental AD group. In addition, Parkin expression was significantly increased at 6, 9, and 12 months-of-age in the experimental AD group. The expression level of Miro decreased significantly at 6, 9, and 12 months-of-age in the experimental AD group. These results suggest that the PINK1/Parkin/Miro pathway is activated in response to mitochondrial damage; however, accumulation of autophagosomes in the experimental AD group at 9 months-of-age, observed via TEM, indicate that

these damaged mitochondria are not effectively cleared. A potential mechanism of this accumulation is disruption of the lysosomal degradation pathway. Thus, Western blot was used to measure the autophagy marker LC3, the autophagy substrate P62, and the mitochondrial outer membrane marker Tom20 (Chai et al. 2018). The results showed that LC3 expression was significantly increased in the experimental AD group at 6, 9, and 12 months-of-age. P62 was also significantly increased in the experimental AD group at 6, 9, and 12 months-of-age, although the levels trended toward a decrease from 6 to 12 months-of-age. There was no significant difference in Tom20 expression between the experimental AD groups. Collectively, these results suggest that mitochondrial damage gradually increases with age, and autophagy and mitophagy activity also increase while lysosomal degradation is inhibited, resulting in the accumulation of damaged mitochondria and cell death.

Studies have shown that mitochondrial damage decreases ATP production in patients with AD (Patro et al. 2021). A recent study found that ATP release in the hippocampus of APP/PS1 double-transgenic mice decreases at 6 months-of-age. In addition, A β levels were increased, and the activities of the APP cleaving enzymes α -secretase and β -secretase were decreased. Increased enzymatic activity and reduced ATP production are indicative of mitochondrial dysfunction and are associated with the onset and progression of AD (Benito-Cuesta et al. 2021). In vitro studies have shown that ATP and ADP can reduce misfolding of A β , providing a link between metabolic dysfunction-related decreases in ATP production and the onset and progression of AD (Croteau et al. 2018). To further characterize the relationship between ATP and related metabolic pathways in the hippocampus of APP/PS1 mice, GC/MS was used to detect changes in levels of metabolites in the hippocampus.

The present study showed that metabolites in APP/PS1 mice were high at 6 and 9 months of age, and low at 12 months-of-age. This dynamic change may be due to compensatory metabolic methods that are adapted to meet the energy requirements of the brain in response to reduced ATP production caused by mitochondrial damage in AD. Consistent with previous studies, mitochondrial damage in APP/PS1 mice was aggravated at 6 and 9 months of age, concomitant with observed alterations in metabolites as a result of compensatory metabolic alterations. However, it is possible that the APP/PS1 mice were unable to sustain this proposed compensatory metabolic alteration at 12 months-of-age, due to irreparable mitochondrial damage and ageing. Interestingly, the metabolic levels of citrate and succinate, which are directly related to ATP production, were both increased during this dynamic change.

Citric acid and succinic acid play key roles in the TCA cycle. The glucose metabolic intermediate pyruvate is

produced by glycolysis, fatty acid conversion, and gluconeogenesis and is converted to acetyl-CoA and then citric acid, releasing reducing H ions that are used to generate ATP. Citric acid is converted into isocitrate, α -ketoglutarate, and then succinyl-CoA to generate succinate, which releases reducing H ions to ultimately generate ATP (Martinez-Reyes, & Chandel, 2020). Succinic acid is converted to fumaric acid, malic acid, and oxaloacetic acid to complete the TCA cycle. Studies have shown that elevated levels of succinate in the intestinal lumen are associated with microbial disturbances, malnutrition, and inflammatory bowel disease (Yin et al. 2014). Citric acid has previously been used as a predictive marker for early diabetic nephropathy (Gao et al. 2018). These studies agree with the results of the present study, where changes in key metabolites of the TCA cycle were associated with the onset and progression of disease. High levels of citric acid and succinic acid were observed in the present study. We speculate that high citrate levels reflect a compensatory metabolic mechanism that is activated to produce sufficient pyruvate. When large consumption or insufficient production of intermediate enzymes, such as acetyl-CoA, isocitrate dehydrogenase, and α -ketoglutarate dehydrogenase, occurs concomitantly, citrate gradually accumulates. Similar changes resulting in high levels of succinate may be due to a similar process, whereby depletion or insufficient supplementation of succinate dehydrogenase, fumarate, and malate dehydrogenase leads to succinate accumulation.

5 Conclusion

There is a positive correlation between the decline of learning and memory in APP/PS1 mice and mitochondrial damage in the hippocampus. Mitochondrial dysfunction leads to insufficient ATP production and further aggravates mitochondrial damage. As seen in Fig. 5, the present study shows that in order to meet energy needs, the body upregulates the TCA cycle to generate ATP; however, if mitochondrial damage is present, the TCA cycle is unable to generate sufficient levels of intermediate enzymes for metabolite conversion, the TCA metabolites citric acid and succinic acid accumulate, and ATP production decreases. The body cannot conduct effective life activities, including the clearance of A β and damaged mitochondria, which eventually leads to the development of AD (Fig. 5). Here, the dynamic relationships between AD, mitochondrial damage, and energy metabolism during ageing were explored, and their mechanisms of interaction were clarified, providing novel ideas and targets for the treatment of AD.

Future studies are necessary to verify the observed dynamic changes in citric acid and succinic acid in the TCA

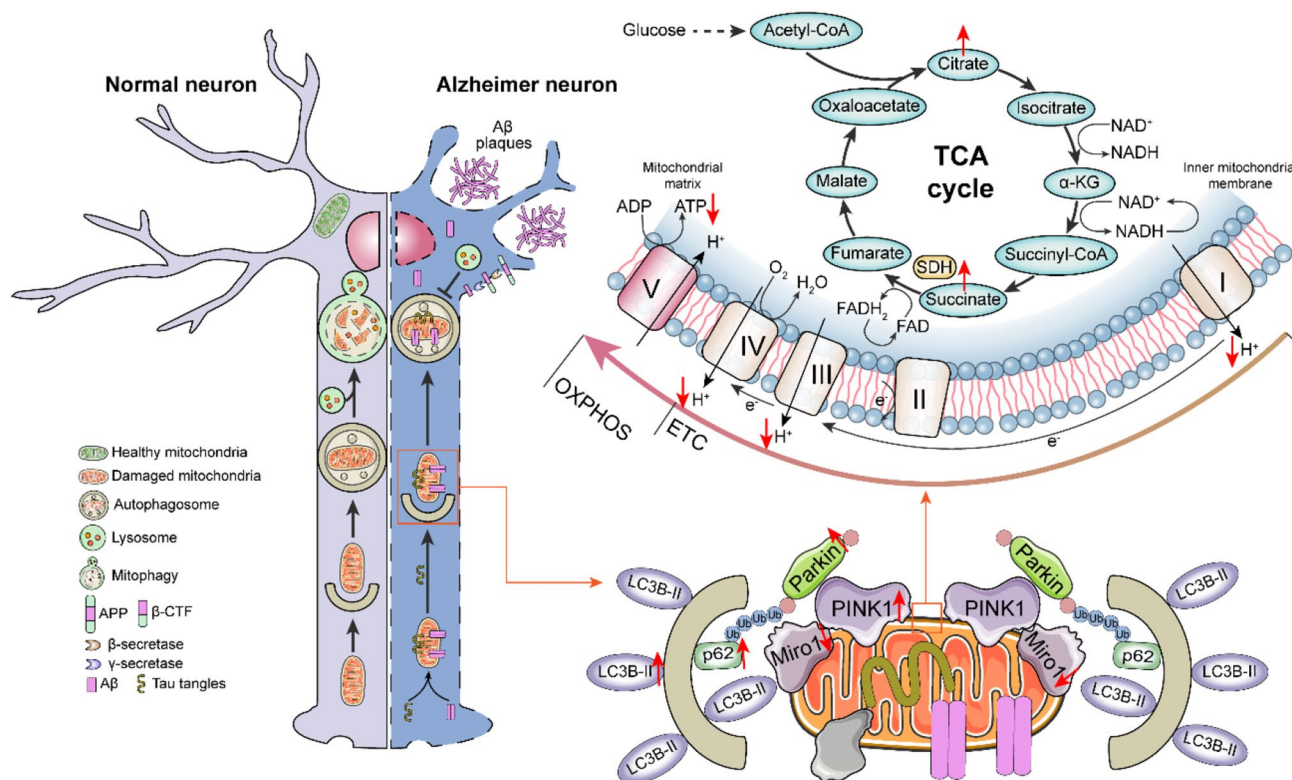


Fig. 5 Mitochondrial damage and associated metabolic imbalances in APP/PS1 mice. The study found that in the early stage of AD model mice, the damaged mitochondria in the hippocampus lead to the enhancement of mitochondrial autophagy and the overconsumption of

cycle in AD and explore the potential of targeting the TCA cycle and ATP production as a therapeutic strategy for AD.

Acknowledgements The authors thank all APP/PS1 mice who participated and continue to contribute to ongoing research. This work was supported by The Performance Incentive Guidance for Scientific Research Institution of Chongqing (No. cstc2020jxjl130013); and the Fundamental Research Funds for the Central University (No. 2019CDYGD002).

Author contributions LSJ and LY were responsible for study design, statistical analysis and manuscript preparation. LSJ, XXM, ZFL, LGX, PY and LXJ conducted experiments. WYY, FJN and LX analyzed data. LSJ, ZX and LY wrote the manuscript. All authors read and approved the manuscript.

Data availability The availability of all data presented in this study is from authors upon request.

Declarations

Competing interests The authors declare that they have no known competing financial interests or personal relationships that could have appeared to influence the work reported in this paper.

Ethics approval and consent to participate Experiments in mice were

performed under Ethical code: CZLS2022061-A of Chongqing University Cancer Hospital.

References

- Akbari, M., Kirkwood, T. B. L., & Bohr, V. A. (2019). Mitochondria in the signaling pathways that control longevity and health span. *Ageing Research Reviews*, *54*, 100940. <https://doi.org/10.1016/j.arr.2019.100940>.
- An, Y., et al. (2018). Evidence for brain glucose dysregulation in Alzheimer's disease. *Alzheimers Dement*, *14*, 318–329. <https://doi.org/10.1016/j.jalz.2017.09.011>.
- Babcock, K. R., Page, J. S., Fallon, J. R., & Webb, A. E. (2021). Adult hippocampal neurogenesis in aging and Alzheimer's Disease. *Stem Cell Reports*, *16*, 681–693. <https://doi.org/10.1016/j.stemcr.2021.01.019>.
- Barthelemy, N. R., et al. (2020). A soluble phosphorylated tau signature links tau, amyloid and the evolution of stages of dominantly inherited Alzheimer's disease. *Nature Medicine*, *26*, 398–407. <https://doi.org/10.1038/s41591-020-0781-z>.
- Benito-Cuesta, I., Ordonez-Gutierrez, L., & Wandosell, F. (2021). AMPK activation does not enhance autophagy in neurons in contrast to MTORC1 inhibition: Different impact on beta-amyloid clearance. *Autophagy*, *17*, 656–671. <https://doi.org/10.1080/1548627.2020.1728095>.
- Bharat, V., & Wang, X. (2020). Precision Neurology for Parkinson's Disease: Coupling Miro1-Based diagnosis with Drug Discovery.

- Movement Disorders*, 35, 1502–1508. <https://doi.org/10.1002/mds.28194>.
- Butterfield, D. A., & Halliwell, B. (2019). Oxidative stress, dysfunctional glucose metabolism and Alzheimer disease. *Nature Reviews Neuroscience*, 20, 148–160. <https://doi.org/10.1038/s41583-019-0132-6>.
- Cai, Q., & Jeong, Y. Y. (2020). Mitophagy in Alzheimer's Disease and other Age-Related neurodegenerative Diseases. *Cells*, 9, <https://doi.org/10.3390/cells9010150>.
- Cen, X., et al. (2020). Pharmacological targeting of MCL-1 promotes mitophagy and improves disease pathologies in an Alzheimer's disease mouse model. *Nature Communications*, 11, 5731. <https://doi.org/10.1038/s41467-020-19547-6>.
- Chai, Y. L., et al. (2018). Mitochondrial translocation of the outer membrane alterations may underlie dysfunctional oxidative phosphorylation in Alzheimer's Disease. *Journal Of Alzheimer'S Disease*, 61, 793–801. <https://doi.org/10.3233/JAD-170613>.
- Croteau, E., et al. (2018). Ketogenic medium chain triglycerides increase Brain Energy Metabolism in Alzheimer's Disease. *Journal Of Alzheimer'S Disease*, 64, 551–561. <https://doi.org/10.3233/JAD-180202>.
- Eysert, F., Kinoshita, P. F., Mary, A., Vaillant-Beuchot, L., Checler, F., & Chami, M. (2020). Molecular Dysfunctions of Mitochondria-Associated membranes (MAMs) in Alzheimer's Disease. *International Journal Of Molecular Sciences*, 21, <https://doi.org/10.3390/ijms21249521>.
- Fang, E. F., et al. (2019). Mitophagy inhibits amyloid-beta and tau pathology and reverses cognitive deficits in models of Alzheimer's disease. *Nature Neuroscience*, 22, 401–412. <https://doi.org/10.1038/s41593-018-0332-9>.
- Ferrari, C., & Sorbi, S. (2021). The complexity of Alzheimer's disease: An evolving puzzle. *Physiological Reviews*, 101, 1047–1081. <https://doi.org/10.1152/physrev.00015.2020>.
- Gao, H., et al. (2018). Quantitative GC-MS assay of citric acid from humans and db/db mice blood serum to assist the diagnosis of diabetic nephropathy. *Journal Of Chromatography. B, Analytical Technologies In The Biomedical And Life Sciences*, 1077–1078, 28–34. <https://doi.org/10.1016/j.jchromb.2017.12.021>.
- Hou, Y., et al. (2019). Ageing as a risk factor for neurodegenerative disease. *Nat Rev Neurol*, 15, 565–581. <https://doi.org/10.1038/s41582-019-0244-7>.
- Imai, Y. (2020). PINK1-Parkin signaling in Parkinson's disease: Lessons from Drosophila. *Neuroscience Research*, 159, 40–46. <https://doi.org/10.1016/j.neures.2020.01.016>.
- Jadiya, P., et al. (2019). Impaired mitochondrial calcium efflux contributes to disease progression in models of Alzheimer's disease. *Nature Communications*, 10, 3885. <https://doi.org/10.1038/s41467-019-11813-6>.
- Jeong, S. (2017). Molecular and Cellular basis of Neurodegeneration in Alzheimer's Disease. *Molecules And Cells*, 40, 613–620. <https://doi.org/10.14348/molcells.2017.0096>.
- John, A., & Reddy, P. H. (2021). Synaptic basis of Alzheimer's disease: Focus on synaptic amyloid beta, P-tau and mitochondria. *Ageing Research Reviews*, 65, 101208. <https://doi.org/10.1016/j.arr.2020.101208>.
- Kane, L. A., & Youle, R. J. (2011). PINK1 and parkin flag miro to direct mitochondrial traffic. *Cell*, 147, 721–723. <https://doi.org/10.1016/j.cell.2011.10.028>.
- Li, Q., Liu, Y., & Sun, M. (2017). Autophagy and Alzheimer's Disease. *Cellular And Molecular Neurobiology*, 37, 377–388. <https://doi.org/10.1007/s10571-016-0386-8>.
- Liu, S., et al. (2012). Parkinson's disease-associated kinase PINK1 regulates Miro protein level and axonal transport of mitochondria. *Plos Genetics*, 8, e1002537. <https://doi.org/10.1371/journal.pgen.1002537>.
- Lonnemann, N., et al. (2020). The NLRP3 inflammasome inhibitor OLT1177 rescues cognitive impairment in a mouse model of Alzheimer's disease. *Proc Natl Acad Sci U S A*, 117, 32145–32154. <https://doi.org/10.1073/pnas.2009680117>.
- Lopez-Domenech, G., et al. (2018). Miro proteins coordinate microtubule- and actin-dependent mitochondrial transport and distribution. *Embo Journal*, 37, 321–336. <https://doi.org/10.15252/embj.201696380>.
- Lopez-Domenech, G., et al. (2021). Loss of neuronal Miro1 disrupts mitophagy and induces hyperactivation of the integrated stress response. *Embo Journal*, 40, e100715. <https://doi.org/10.15252/embj.2018100715>.
- Luo, R., et al. (2020). Activation of PPARA-mediated autophagy reduces Alzheimer disease-like pathology and cognitive decline in a murine model. *Autophagy*, 16, 52–69. <https://doi.org/10.1080/15548627.2019.1596488>.
- Mahajan, U. V., et al. (2020). Dysregulation of multiple metabolic networks related to brain transmethylation and polyamine pathways in Alzheimer disease: A targeted metabolomic and transcriptomic study. *Plos Medicine*, 17, e1003012. <https://doi.org/10.1371/journal.pmed.1003012>.
- Martinez-Reyes, I., & Chandel, N. S. (2020). Mitochondrial TCA cycle metabolites control physiology and disease. *Nature Communications*, 11, 102. <https://doi.org/10.1038/s41467-019-13668-3>.
- Nikolac Perkovic, M., et al. (2021). Epigenetics of Alzheimer's Disease. *Biomolecules*, 11, <https://doi.org/10.3390/biom11020195>.
- Panchal, K., & Tiwari, A. K. (2021). Miro (mitochondrial rho GTPase), a key player of mitochondrial axonal transport and mitochondrial dynamics in neurodegenerative diseases. *Mitochondrion*, 56, 118–135. <https://doi.org/10.1016/j.mito.2020.10.005>.
- Park, M. W., et al. (2021). NOX4 promotes ferroptosis of astrocytes by oxidative stress-induced lipid peroxidation via the impairment of mitochondrial metabolism in Alzheimer's diseases. *Redox Biology*, 41, 101947. <https://doi.org/10.1016/j.redox.2021.101947>.
- Patro, S., et al. (2021). ATP synthase and mitochondrial bioenergetics dysfunction in Alzheimer's Disease. *International Journal Of Molecular Sciences*, 22, <https://doi.org/10.3390/ijms222011185>.
- Perez Ortiz, J. M., & Swerdlow, R. H. (2019). Mitochondrial dysfunction in Alzheimer's disease: Role in pathogenesis and novel therapeutic opportunities. *British Journal Of Pharmacology*, 176, 3489–3507. <https://doi.org/10.1111/bph.14585>.
- Pradeepkiran, J. A., & Reddy, P. H. (2020). Defective mitophagy in Alzheimer's disease. *Ageing Research Reviews*, 64, 101191. <https://doi.org/10.1016/j.arr.2020.101191>.
- Quinn, P. M. J., Moreira, P. I., Ambrosio, A. F., & Alves, C. H. (2020). PINK1/PARKIN signalling in neurodegeneration and neuroinflammation. *Acta Neuropathol Commun*, 8, 189. <https://doi.org/10.1186/s40478-020-01062-w>.
- Reddy, P. H., & Oliver, D. M. (2019). Amyloid Beta and phosphorylated Tau-Induced defective autophagy and Mitophagy in Alzheimer's Disease. *Cells*, 8, <https://doi.org/10.3390/cells8050488>.
- Reddy, P. H., et al. (2018). Mutant APP and amyloid beta-induced defective autophagy, mitophagy, mitochondrial structural and functional changes and synaptic damage in hippocampal neurons from Alzheimer's disease. *Human Molecular Genetics*, 27, 2502–2516. <https://doi.org/10.1093/hmg/ddy154>.
- Scheltens, P., et al. (2021). Alzheimer's disease. *Lancet*, 397, 1577–1590. [https://doi.org/10.1016/S0140-6736\(20\)32205-4](https://doi.org/10.1016/S0140-6736(20)32205-4).
- Shoshan-Barmatz, V., Nahon-Crystal, E., Shteiufer-Kuzmine, A., & Gupta, R. (2018). VDAC1, mitochondrial dysfunction, and Alzheimer's disease. *Pharmacological Research*, 131, 87–101. <https://doi.org/10.1016/j.phrs.2018.03.010>.
- Sun, K., Jing, X., Guo, J., Yao, X., & Guo, F. (2021). Mitophagy in degenerative joint diseases. *Autophagy*, 17, 2082–2092. <https://doi.org/10.1080/15548627.2020.1822097>.

- Swerdlow, R. H. (2018). Mitochondria and mitochondrial cascades in Alzheimer's Disease. *Journal Of Alzheimer'S Disease*, *62*, 1403–1416. <https://doi.org/10.3233/JAD-170585>.
- Tang, B. L. (2020). Glucose, glycolysis, and neurodegenerative diseases. *Journal Of Cellular Physiology*, *235*, 7653–7662. <https://doi.org/10.1002/jcp.29682>.
- Tolar, M., Abushakra, S., & Sabbagh, M. (2020). The path forward in Alzheimer's disease therapeutics: Reevaluating the amyloid cascade hypothesis. *Alzheimers Dement*, *16*, 1553–1560. <https://doi.org/10.1016/j.jalz.2019.09.075>.
- Velazquez, R., et al. (2019). Lifelong choline supplementation ameliorates Alzheimer's disease pathology and associated cognitive deficits by attenuating microglia activation. *Aging Cell*, *18*, e13037. <https://doi.org/10.1111/accel.13037>.
- Wang, N., et al. (2020a). PINK1: The guard of mitochondria. *Life Sciences*, *259*, 118247. [10.1016/j.lfs.2020a.118247](https://doi.org/10.1016/j.lfs.2020a.118247).
- Wang, W., Zhao, F., Ma, X., Perry, G., & Zhu, X. (2020b). Mitochondria dysfunction in the pathogenesis of Alzheimer's disease: Recent advances. *Mol Neurodegener*, *15*, 30. [10.1186/s13024-020-00376-6](https://doi.org/10.1186/s13024-020-00376-6).
- Weidling, I. W., & Swerdlow, R. H. (2020). Mitochondria in Alzheimer's disease and their potential role in Alzheimer's proteostasis. *Experimental Neurology*, *330*, 113321. <https://doi.org/10.1016/j.expneurol.2020.113321>.
- Xiong, X., et al. (2020). Study of mitophagy and ATP-related metabolomics based on beta-amyloid levels in Alzheimer's disease. *Experimental Cell Research*, *396*, 112266. <https://doi.org/10.1016/j.yexcr.2020.112266>.
- Yin, F., Boveris, A., & Cadenas, E. (2014). Mitochondrial energy metabolism and redox signaling in brain aging and neurodegeneration. *Antioxidants & Redox Signaling*, *20*, 353–371. <https://doi.org/10.1089/ars.2012.4774>.
- Zhao, Y., Zeng, C. Y., Li, X. H., Yang, T. T., Kuang, X., & Du, J. R. (2020). Klotho overexpression improves amyloid-beta clearance and cognition in the APP/PS1 mouse model of Alzheimer's disease. *Aging Cell*, e13239. <https://doi.org/10.1111/accel.13239>.
- Zhou, F., et al. (2020). Enhanced autophagic retrograde axonal transport by dynein intermediate chain upregulation improves Abeta clearance and cognitive function in APP/PS1 double transgenic mice. *Aging (Albany NY)*, *12*, 12142–12159. <https://doi.org/10.18632/aging.103382>.
- Alzheimer's disease facts and figures. *Alzheimers Dement* *18*, 700–789 doi:<https://doi.org/10.1002/alz.12638>

Publisher's Note Springer Nature remains neutral with regard to jurisdictional claims in published maps and institutional affiliations.

Springer Nature or its licensor (e.g. a society or other partner) holds exclusive rights to this article under a publishing agreement with the author(s) or other rightsholder(s); author self-archiving of the accepted manuscript version of this article is solely governed by the terms of such publishing agreement and applicable law.